Journal of Applied Fluid Mechanics, Vol. 11, No. 5, pp. 1173-1183, 2018.
Available online at www.jafmonline.net, ISSN 1735-3572, EISSN 1735-3645.
DOI: 10.29252/jafm.11.05.38039

Effect of Viscous Gas on Stability of the Electrified Liquid Sheet

R. Duan[1], Y. Liu[1], D. Wang [1], Z. Wang [1], L. Liu [1†] and Y. Zhang[2]

[1]*School of Energy and Environmental Engineering, Hebei University of Technology, Tianjin, 300401, China*
[2]*Department of Civil Engineering, Nanyang Institute of Technology, Nanyang, 473004, China*

[†]*Corresponding Author Email: liuliansheng@hebut.edu.cn*

(Received May 24, 2017; accepted April 15, 2018)

ABSTRACT

An electrified liquid sheet was investigated by the linear analysis method. The sheet was injected into a dielectric viscous gas bounded by two horizontal parallel flat plates with a transverse electric field. To take into account the gas boundary layer thickness, the velocity profile of the liquid sheet must be considered and derived. By analyzing the liquid and gas domain, the relation between the growth rate and the wavenumbers for electrified liquid sheets was derived, and solved using the spectral method whose accuracy is higher than those of the finite element method and the finite difference method. Two modes, namely the sinuous mode and varicose mode were also investigated. The results revealed that the maximum growth rate of the sinuous disturbance wave is greater than that of the varicose one for the electrified liquid sheet. Moreover, the effects of the electrified Euler number and other parameters on the instability of the electrified liquid sheets have been tested. It is found that the growth rate is faster for an electrified liquid sheet than a non-electrified one. The electrical Euler number, the liquid Reynolds number, the Weber number and the momentum flux ratio can promote the breakup of a liquid sheet. However, the increase in the ratio *l* of the distance between the liquid sheet and flat plate to the liquid sheet thickness has an opposite influence with the other parameters.

Keywords: Instability; Electrified planar liquid sheet; Velocity profile; Spectral method; Linear analysis.

NOMENCLATURE

U	velocity along the x-axis	k_d	dominant wavenumber
V	velocity along y-axis		
ρ_1	liquid density	$\bar{U}_1$	liquid mean velocity
ρ_2	gas density	We	Weber number
p	pressure perturbation	σ	liquid surface tension
μ	viscosity	Re_1	liquid Reynolds number
h	half-thickness of liquid sheet	Re_2	gas Reynolds number
δ	local air boundary layer thickness	ω	growth rate of perturbation
u	perturbation along *x*-axis	ψ	velocity potential
v	perturbation along *y*-axis	α	phase parameter
d_{ij}	rate of deformation tensor	t	time
η	displacements from the equilibrium position		

1. INTRODUCTION

Electrospraying and electrospinning have been extensively emphasized in the past decades owing to many applications in industry, agriculture, medical care and others. The electric fields are used to control the track and size of the droplets, which are sensitive to the applied voltage (Yang (2013), Duan (2014)).

The instability of the electrified liquid sheets has been a subject of the numerous investigations. Since the first studies by Savart (1833), the breakup of the flat sheets has been investigated by numerous other researchers. Squire (1953) and Hagerty *et al*. (1955) investigated a uniform thickness inviscid liquid sheet in an inviscid gas environment, and analyzed the characteristics of the sinuous (Fig.1a) and varicose (Fig.1b) modes. Their results showed that the surface tension always tended to damp out any disturbances. The aerodynamic force caused by the interaction between the liquid sheet and the ambient gas were responsible for the instability, which were in good agreement with the experiment results. Ibrahim (1998) studied the evolution of the antisymmetrical and symmetrical disturbances of a moving viscous liquid sheet in a quiescent inviscid gas using the spatial instability theory. The breakup of a conical liquid sheet under the combined influence of the sinuous and varicose modes at the liquid-gas interfaces was experimentally and theoretically investigated (Fu *et al*. 2010). It is reported that the disturbance growth rate of the varicose mode is more stable than that of the sinuous one. The conclusion was successfully confirmed by their experiment. Moreover, the breakup mechanisms of the Newtonian liquid sheets have been performed by many theoretical and experimental investigations (Yang (2013), Li (1991), Lin (1990)).

In the theoretical works cited above, the instability of a liquid sheet in an inviscid gas medium was performed (Ibrahim (1998), Lin (1990), Dombrowski (1963), Taylor (1959), Li (1993)). However, the effect of the viscous gas surroundings on the breakup of the liquid sheets should be considered in practice. Because a liquid sheet issued from the nozzle with a nonuniform velocity. It is necessary to investigate the instability behavior of a liquid sheet with the nonuniform velocity profile. Tomotika (1935) considered the solution to include the effect of the viscous surroundings. Their solutions are often applied as the theoretical solution of the practical problems even now. Henceforth, many investigations on the instability of the liquid sheets have been performed. Teng *et al*. (1997) performed on a specific wall bounded configuration with the viscosity and velocity profiles of the surrounding air using the linear stability analysis. By considering the inviscid liquid sheet emanated from a nozzle into an otherwise quiescent inviscid gas, Ibrahim (1998) compared the sheets with the uniform velocity profile with that with the parabolic velocity profile. The conclusion is that the parabolic velocity profile reduced the liquid-gas relative velocity across the interface and decreased the aerodynamic instability. Therefore, the liquid sheet with the parabolic velocity profile is more stable than that with the uniform profile. The effect of a parabolic velocity profile moving through the viscous ambient gas with velocity on the liquid sheet instability was experimentally and theoretically investigated (Lozano *et al*. 2001). Their results found that the air velocity being constant, the disturbance growth rate decreased with the increase of the liquid velocity. However, the velocity profiles were not derived in detail.

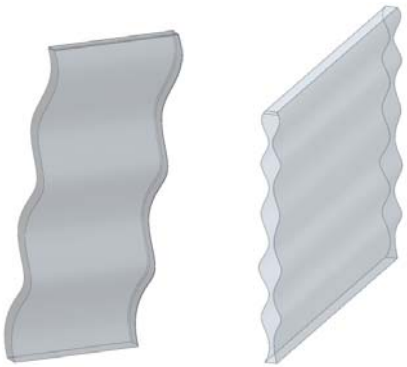

(a) the sinuous mode　　（b）the varicose mode

Fig. 1. Schematic diagram of a liquid sheet

The effect of the Electric fields on the breakup of the liquid sheet was investigated by using the experimental and theoretical methods (Georgiou (1991), Lee (2002),Tilley (2001), Savetta-seranee (2003), Papageorgiou (2004), Ozen (2006)). Grandison (2007) considered the waves propagating on the surface of a two-dimensional inviscid liquid layer, bounded by a second incompressible inviscid fluid, and in the presence of an electric field. It was found that the electric field competed directly with the Kelvin-Helmholtz instability. They had the same shortwave behavior but contributed the opposite signs to the growth rate.

The objective of this paper is to investigate the temporal instability of the electrified liquid sheets in a surrounding viscous gas. The gas is bounded by two horizontal parallel electrodes. Firstly, the velocity profile of the liquid sheets is derived. Secondly, the dispersion relation between the growth rate and the wavenumbers for the electrified liquid sheets are also derived in detail. Finally, the differences between the instability of sinuous and the varicose disturbances, and the effects of the electric fields on the instability of the liquid sheets are also investigated.

2. ELECTRIFIED LIQUID SHEET MODEL

The Fig. 2 shows the model of the constant density fluid sheet surrounded by a viscous gas with a thickness of 2h. The gas is bounded by two horizontal parallel electrodes located at an equidistance of (δ+h) from the centerline of the liquid sheet. The inner liquid has a high electric conductivity, and the outer gas is an insulating dielectric. The centerline velocity of the liquid sheet is $\overline{U}_1$. The direction of the liquid sheet parallels is in the x-direction.

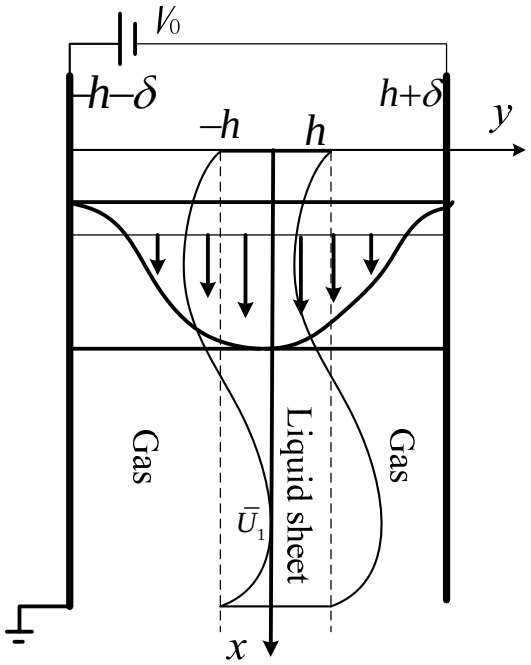

Fig. 2. Sketch of the flow configuration

2.1 Base Flow Velocity Profile

The governing equations for the liquid sheets and viscous gas consist of the conservation laws of the mass and momentum, as follows

$$\frac{\partial U_\alpha}{\partial x}+\frac{\partial V_\alpha}{\partial y}=0 \tag{1}$$

$$\begin{aligned}&\rho_\alpha\left(\frac{\partial U_\alpha}{\partial t}+U_\alpha\frac{\partial U_\alpha}{\partial x}+V_\alpha\frac{\partial U_\alpha}{\partial y}\right)\\&=-\frac{\partial p_\alpha}{\partial x}+\mu_\alpha\left(\frac{\partial^2 U_\alpha}{\partial x^2}+\frac{\partial^2 U_\alpha}{\partial y^2}\right)\end{aligned} \tag{2}$$

where subscript α=1, 2 represents the liquid and gas phase, respectively. ρ denotes the density, U denotes the velocity along the x-axis. V is the velocity along y-axis, and μ is the viscosity.

The liquid sheet and gas are steady flows $\frac{\partial U_\alpha}{\partial t}=0$. The liquid and gas velocities are independent of x-axis, $\frac{\partial U_\alpha}{\partial x}=0$. V denotes velocity along y-axis $V_\alpha=0$. Equation (2) yields

$$U_1=A_1+B_1y+\frac{1}{2\mu_1}\frac{\partial p_1}{\partial x}y^2,-h\le y\le h \tag{3}$$

$$U_2=A_2+B_2y+\frac{1}{2\mu_2}\frac{\partial p_2}{\partial x}y^2,h\le y\le h+\delta \tag{4}$$

$$\begin{aligned}&U_2=A_2-B_2y+\frac{1}{2\mu_2}\frac{\partial p_2}{\partial x}y^2,\\&-(h+\delta)\le y\le -h\end{aligned} \tag{5}$$

The unknown coefficients A, B and liquid and gas velocities U at the unperturbed interface are calculated by the following boundary conditions (Lozano, 2001):

(a) the tangential viscous stresses balance at the unperturbed interface, $y=\pm h$.

(b) the central velocity of the liquid sheet is equal to $\bar{U}_1$, $y=0$.

(c) the air velocities are equal to zero at the electrodes, $y=\pm(\delta+h)$.

(d) the air pressure gradient is equal to the liquid pressure gradient, $y=\pm h$.

(e) the gas and liquid velocities are equal at the unperturbed interface, $y=\pm h$

$$A_1=\bar{U}_1 \tag{6}$$

$$\left.\frac{\partial p_1}{\partial x}\right|_{y=h}=\left.\frac{\partial p_2}{\partial x}\right|_{y=h} \tag{7}$$

$$B_1=\frac{-\bar{U}_1-\frac{1}{2\mu_1}\left.\frac{\partial p_1}{\partial x}\right|_{y=h}h^2}{h+\frac{\mu_1}{\mu_2}\delta} \tag{8}$$

$$A_2=\frac{\frac{\mu_1}{\mu_2}\bar{U}_1+\frac{1}{2\mu_2}\left.\frac{\partial p_1}{\partial x}\right|_{y=h}h^2}{h+\frac{\mu_1}{\mu_2}\delta}(\delta+h) \tag{9}$$

$$\left.\frac{\partial p_2}{\partial x}\right|_{y=h}=\frac{-2\mu_2\bar{U}_1}{(\frac{\mu_2}{\mu_1}-1)h^2+(\delta+h)^2} \tag{10}$$

$$\left.\frac{\partial p_2}{\partial x}\right|_{y=h+\delta}=0 \tag{11}$$

2.2 Liquid Phase

The governing equations of the liquid sheets consist of the conservation laws of the mass and momentum, as follows:

$$\frac{\partial u_1}{\partial x}+\frac{\partial v_1}{\partial y}=0 \tag{12}$$

$$\rho_1\left(\frac{\partial u_1}{\partial t}+U_1\frac{\partial u_1}{\partial x}+v_1\frac{\partial U_1}{\partial y}\right) = -\frac{\partial p_1}{\partial x}+\mu_1\left(\frac{\partial^2 u_1}{\partial x^2}+\frac{\partial^2 u_1}{\partial y^2}\right) \tag{13}$$

$$\rho_1\left(\frac{\partial v_1}{\partial t}+U_1\frac{\partial v_1}{\partial x}\right) = -\frac{\partial p_1}{\partial y}+\mu_1\left(\frac{\partial^2 v_1}{\partial x^2}+\frac{\partial^2 v_1}{\partial y^2}\right) \tag{14}$$

The boundary conditions at the interface $y=\pm(h+\eta(x,t))$ are linearized about $y=\pm h$ and only the first-order perturbation are retained, where $\eta_+(x,t)$ and $\eta_-(x,t)$ are the upper and lower interface displacements from the equilibrium position. The boundary conditions are as follows:

Continuity of *u*

$$\mu_1(\pm h)+\eta_\pm\frac{dU_1(\pm h)}{\partial y} = \mu_2(\pm h)+\eta_\pm\frac{dU_2(\pm h)}{dy} \tag{15}$$

Continuity of *v*

$$v_1(\pm h)=v_2(\pm h) \tag{16}$$

Continuity of tangential stress

$$\mu_1\left(\frac{\partial u_1(\pm h)}{\partial y}+\frac{\partial v_1(\pm h)}{\partial x}\right) = \mu_2\left(\frac{\partial u_2(\pm h)}{\partial y}+\frac{\partial v_2(\pm h)}{\partial x}\right) \tag{17}$$

Normal stress jump

$$p_1(\pm h)-2\mu_1\frac{\partial v_1(\pm h)}{\partial y}=p_2(\pm h) -2\mu_2\frac{\partial v_2(\pm h)}{\partial y}-\sigma\frac{\partial^2\eta_\pm}{\partial x^2}-\frac{1}{2}\varepsilon_0 E^2 \tag{18}$$

Kinematic condition

$$v_1=\frac{\partial\eta_\pm}{\partial t}+U_1\frac{\partial\eta_\pm}{\partial x} \tag{19}$$

2.3 Gas Phase

In this paper, the liquid sheet is surrounded by a viscous gas. The gas is bounded by two horizontal parallel electrodes located at an equidistance of ($h+\delta$) from the centerline of the liquid sheet to the horizontal parallel electrodes. The governing equations for the viscous gas are the conservation laws of the mass and momentum, as follows

$$\frac{\partial u_2}{\partial x}+\frac{\partial v_2}{\partial y}=0 \tag{20}$$

$$\rho_2\left(\frac{\partial u_2}{\partial t}+U_2\frac{\partial u_2}{\partial x}\right) = -\frac{\partial p_2}{\partial x}+\mu_2\left(\frac{\partial^2 u_2}{\partial x^2}+\frac{\partial^2 u_2}{\partial y^2}\right) \tag{21}$$

$$\rho_2\left(\frac{\partial v_2}{\partial t}+U_2\frac{\partial v_2}{\partial x}\right) = -\frac{\partial p_2}{\partial y}+\mu_2\left(\frac{\partial^2 v_2}{\partial x^2}+\frac{\partial^2 v_2}{\partial y^2}\right) \tag{22}$$

Similar to the liquid phase, the boundary conditions of the viscous gas are as follows

Continuity of *u*

$$u_2(\pm b)=0 \tag{23}$$

Continuity of *v*

$$v_2(\pm b)=0 \tag{24}$$

Kinematic condition

$$v_2=\frac{\partial\eta_\pm}{\partial t}+U_2\frac{\partial\eta_\pm}{\partial x} \tag{25}$$

where $b=h+\delta$

2.4 Electrical Field

In electriostatic, the electrical potential perturbation V_e satisfies the Laplace equation (Li (2007))

$$\nabla^2 V_e=0 \tag{26}$$

The electric boundary conditions are the electrical potential which is V_0 at the liquid sheet and is zero at the electrode:

$$V_e\big|_{y=h+\eta}=V_0 \tag{27}$$

$$V_e\big|_{y=\delta+h}=0 \tag{28}$$

The electric field intensity is

$$E=-\nabla V_e=\frac{V_0}{h+\delta-\eta} \tag{29}$$

The electric fields are used to increase the disturbance of the liquid sheet.

2.5 Governing Equation

The normal stress jump is continuous at the interface, and the boundary condition can be written as:

$$p_1 - 2\mu_1 \frac{\partial v_1}{\partial y} = p_2 - 2\mu_2 \frac{\partial v_2}{\partial y} \\ -\sigma \frac{\partial^2 \eta}{\partial x^2} - (\frac{1}{2}\varepsilon_0 E^2)_{linear}, \quad y = h + \eta \tag{30}$$

$$p_1 - 2\mu_1 \frac{\partial v_1}{\partial y} = -p_2 - 2\mu_2 \frac{\partial v_2}{\partial y} \\ -\sigma \frac{\partial^2 \eta}{\partial x^2} + (\frac{1}{2}\varepsilon_0 E^2)_{linear}, \quad y = -(h + \eta) \tag{31}$$

where σ is the surface tension, ε_0 is the electrical permittivity, by the electric field intensity (29)

$$E^2 = (\frac{V_0}{h + \delta - \eta}) - (\frac{V_0}{h + \delta})^2 \tag{32}$$

The first term of Eq. (32) on the right is solved by the Taylor Series Expansion,

$$\frac{1}{(h+\delta-\eta)^2} = \frac{1}{(h+\delta)^2} + 2\frac{1}{(h+\delta)^3}\eta + o(y^2) \\ = \frac{1}{(h+\delta)^2} + 2\frac{1}{(h+\delta)^3}\eta \tag{33}$$

$$(\frac{1}{2}\varepsilon_0 E^2)_{linear} = \frac{1}{2}\varepsilon_0 2\frac{V_0^2}{(h+\delta)^3}\eta \\ = \varepsilon_0 \frac{V_0^2}{(h+\delta)^3}\eta \tag{34}$$

The two-dimensional constant-density flow problem can be conveniently solved in terms of the stream function, $\psi(x, y, t)$, formulation ($u = \frac{\partial \psi}{\partial y}, v = -\frac{\partial \psi}{\partial x}$). By the Eqs. (13) and (21), the governing equations can be obtained as:

$$\upsilon_1 \frac{\partial^4 \psi_1}{\partial y^4} - (\omega + ikU_1 + 2\upsilon_1 k^2)\frac{\partial^2 \psi_1}{\partial^2 y} \\ +(ikU_1'' + \omega k^2 + iU_1 k^3 + \upsilon_1 k^4)\psi_1 = 0 \tag{35}$$

and the Eqs. (15-19) of the boundary conditions can be linearized as:

$$\upsilon_2 \frac{\partial^4 \psi_2}{\partial y^4} - (\omega + ikU_2 + 2\upsilon_2 k^2)\frac{\partial^2 \psi_2}{\partial^2 y} \\ +(ikU_2'' + \omega k^2 + iU_2 k^3 + \upsilon_2 k^4)\psi_2 = 0 \tag{36}$$

$$\frac{\partial \psi_1(\pm h)}{\partial x} = \frac{\partial \psi_2(\pm h)}{\partial x} \tag{37}$$

$$v_1(\pm h) = \frac{\partial \eta_\pm}{\partial t} + U_1(\pm h)\frac{\partial \eta_\pm}{\partial x} \tag{38}$$

$$\frac{\partial \psi_1(\pm h)}{\partial y} + \eta_\pm \frac{dU_1(\pm h)}{dy} \\ = \frac{\partial \psi_2(\pm h)}{\partial y} + \eta_\pm \frac{dU_2(\pm h)}{dy} \tag{39}$$

$$\mu_1(\frac{\partial^2 \psi_1(\pm h)}{\partial y^2} - \frac{\partial^2 \psi_1(\pm h)}{\partial x^2}) \\ = \mu_2(\frac{\partial^2 \psi_2(\pm h)}{\partial y^2} - \frac{\partial^2 \psi_2(\pm h)}{\partial x^2}) \tag{40}$$

$$\upsilon_1 \frac{\partial^3 \psi_1(\pm h)}{\partial y^3} - (\upsilon_1 k^2 + \omega \\ +ikU_1(\pm h) + \frac{2k^2\mu_1}{\rho_1})\frac{\partial \psi_1(\pm h)}{\partial y} \\ +ik\frac{\partial U_1(\pm h)}{\partial y}\psi_1(\pm h) = \frac{\rho_2}{\rho_1}\upsilon_2 \\ \frac{\partial^3 \psi_2(\pm h)}{\partial y^3} - (\frac{\rho_2}{\rho_1}\upsilon_2 k^2 + \frac{\rho_2 \omega}{\rho_1} \\ + \frac{\rho_2}{\rho_1}ikU_2(\pm h) + \frac{2k^2\mu_2}{\rho_1})\frac{\partial \psi_2(\pm h)}{\partial y} \\ + \frac{\rho_2}{\rho_1}ik\frac{\partial U_2(\pm h)}{\partial y}\psi_2(\pm h) + \frac{\sigma i k^3 \eta_\pm}{\rho_1} \\ -\frac{1}{\rho_1}\frac{h}{U_1^2} i\frac{\tilde{k}}{h}\varepsilon_0 \frac{V_0^2}{(\pm(h+\delta))^4} h\eta_\pm \tag{41}$$

Equations (35-41) can be expressed as the perturbed functions in a normal mode decomposition:

$$[\psi(x, y, t), p(x, y, t), \gamma_{ij}(x, y, t) \\ , \tau_{ij}(x, y, t), \eta(x, t)] = \\ [\hat{\psi}(y), \hat{p}(y), \hat{\gamma}_{ij}(y), -\hat{\eta}_0]\exp(ikx + \omega t) \tag{42}$$

For convenience, the above governing Eqs. (35-36) can be expressed in the non-dimensional form. For the sinuous mode $\eta_+(x,t) = \eta_-(x,t)$, while for the varicose mode $\eta_+(x,t) = -\eta_-(x,t)$. In this way, we can obtain the Orr-Sommerfeld equations,

$$\frac{1}{Re_1}\tilde{\psi}_1^{iv}-(\tilde{\omega}+i\tilde{k}\tilde{U}_1+\frac{2\tilde{k}^2}{Re_1})\tilde{\psi}_1''+(i\tilde{k}\tilde{U}_1''+\tilde{\omega}\tilde{k}^2+i\tilde{U}_1\tilde{k}^3+\frac{\tilde{k}^4}{Re_1})\tilde{\psi}_1=0 \tag{43}$$

$$\frac{l}{Re_2}\tilde{\psi}_2^{iv}-(\frac{\tilde{\omega}}{\tilde{U}_2}+i\tilde{k}+2\tilde{k}^2\frac{l}{Re_2})\tilde{\psi}_2''+(i\frac{\tilde{k}}{\tilde{U}_2}\tilde{U}_2''+\frac{\tilde{k}^2\tilde{\omega}}{\tilde{U}_2}+i\tilde{k}^3+\frac{l\tilde{k}^4}{Re_2})\tilde{\psi}_2=0 \tag{44}$$

$$Re_2=\frac{U_2\delta\rho_2}{\mu_2},\quad \tilde{k}=kh,\quad \tilde{\eta}_\pm=\frac{\eta_\pm}{h},$$

e $$\tilde{y}=\frac{y}{h},\quad \tilde{U}_1(\tilde{y})=\frac{U_1(\tilde{y})}{\bar{U}_1},\quad \tilde{U}_2(\tilde{y})=\frac{U_2(y)}{\bar{U}_1},$$

$$\tilde{\psi}_1(\tilde{y})=\frac{\psi_1(y)}{\bar{U}_1 h},\tilde{\psi}_2(\tilde{y})=\frac{\psi_2(y)}{U_2\delta},l=\frac{h}{\delta}$$

The non-dimensional boundary conditions (37-41) are as follows

$$\tilde{\psi}_1(\pm1)-\tilde{U}_2 l\tilde{\psi}_2(\pm1)=0 \tag{45}$$

$$i\tilde{k}\tilde{\psi}_1(\pm1)+(\tilde{\omega}+i\tilde{k}\tilde{U}_1(\pm1))\tilde{\eta}_\pm=0 \tag{46}$$

$$\tilde{\psi}_1'(\pm1)-\tilde{U}_2 l\tilde{\psi}_2'(\pm1)+[\tilde{U}_1'(\pm1)-\tilde{U}_2'(\pm1)]\tilde{\eta}_\pm=0 \tag{47}$$

$$\tilde{\psi}_1''(\pm1)+\tilde{k}^2\tilde{\psi}_1(\pm1)-\frac{Re_1}{Re_2}Q\frac{U_2^2}{U_1^2}l^2(\tilde{\psi}_2''(\pm1)+\tilde{k}^2\tilde{\psi}_2(\pm1))+(\tilde{U}_1''(\pm1)-\frac{Re_1}{Re_2}Q\frac{U_2^2}{U_1^2}l\tilde{U}_2''(\pm1))\tilde{\eta}_\pm=0 \tag{48}$$

$$\frac{1}{Re_1}\tilde{\psi}_1'''(\pm1)-(\frac{3\tilde{k}^2}{Re_1}+\tilde{\omega}+i\tilde{k}\tilde{U}_1(\pm1)+)\tilde{\psi}_1'(\pm1)+i\tilde{k}\tilde{U}_1'\tilde{\psi}_1(\pm1)-Q\frac{U_2^2}{U_1^2}\frac{l^2}{Re_2}\tilde{\psi}_2'''(\pm1)+Q\frac{U_2^2}{U_1^2}(\frac{3\tilde{k}^2 l}{Re_2}+\tilde{\omega}l+i\tilde{k}l\tilde{U}_2(\pm1))\tilde{\psi}_2'(\pm1)-Q\frac{U_2^2}{U_1^2}li\tilde{k}\tilde{U}_2'(\pm1)\tilde{\psi}_2(\pm1)\mp\frac{i\tilde{k}^3\tilde{\eta}_\pm}{We}\pm\frac{Eu}{(1+l)^4}i\tilde{k}\tilde{\eta}_\pm=0 \tag{49}$$

$$\tilde{\psi}_2(\pm(1+l))=0 \tag{50}$$

$$\tilde{\psi}_2'(\pm(1+l))=0 \tag{51}$$

where $Q=\frac{\rho_2}{\rho_1}, We=\frac{\rho_1 U_1^2 h}{\sigma}, Eu=\frac{\varepsilon_0 V_0^2}{\rho_1 U_1^2 h^2}$.

The governing equations can be solved by the numerical method. The disturbance growth rate is numerically obtained by the spectral method, the prototype of which is the well-known Fourier method (Orszag (1971), Peyret (2002), Shen (2006)). The accuracy of the spectral method is higher than those of the finite element method and the finite difference method. The Fourier method represents the solution as a truncated series expansion, which solves the periodic problems. For the nonperiodic problems, the Chebyshev and Legendre methods are usually adopted. In this paper, we will solve this problem by the Chebyshev method.

3. RESULTS AND DISCUSSION

In this paper, the effects of the electrified liquid sheet on the disturbance growth rate are investigated. The effect of Various parameters on the instability of the electrified liquid sheets have been tested.

3.1 Comparison of Electrified and Non-Electrified Liquid Sheet

Figure 3(a) shows the effect of the electric fields on the disturbance wave growth rate. The parameters are held constant to be l=1.0, Re_1=510, We=100, Q=0.001, Eu=1.0. It can be seen that all the curves monotonically increase until a maximum value, and subsequently decrease. The maximum value is caused by the electric fields. The disturbance growth rate of the electrified liquid sheet is greater than that of the non-electrified liquid sheet, as shown in Fig. 3(a). The electric fields can accelerate the breakup of the liquid sheet.

For the inspection of Fig. 3(b), the variation of the disturbance growth rate with the wavenumber of electrified liquid sheet for both the sinuous mode and varicose mode, respectively. For these plots, the parameters are hold constant to be l=0.8, Re_1=510, We=100, Q=0.001, Eu=1.0. The disturbance growth rate of the sinuous mode is larger than that of the varicose one, which denotes that the effect of the sinuous disturbance wave on the breakup of the liquid sheets is dominant. The similar conclusions were obtained in the previous investigations (Yang *et al.* (2013), Ibrahim (1998)). For this reason, only the sinuous mode is investigated herein. However, the effects of the velocity profile of the liquid sheet and gas viscosity on the instability of the liquid sheet were neglected in their studies.

3.2 Effect of the Electrical Euler Number

To investigate the effect of the electrical Euler number

on the disturbance wave growth rate, six values are chosen from 0 to 4 with other parameters held constant (l=1, Re_1=510, We=100, Q=0.001 for the electrified liquid sheet, and Eu=0 for the non-electrified liquid sheet). It is well known that the electrical Euler number indicates the strength of the electrical field. Figure 4 (a) demonstrates that the disturbance growth rate increases with the increase of the electrical Euler number. This is because the instability is enhanced by the electrical Euler number. In the terms of physics, the electrical field can provide more energy to promote the electrified liquid sheet breakup. With the electrical Euler number increasing, the maximum growth rate increases, as shown in Fig. 4 (b).

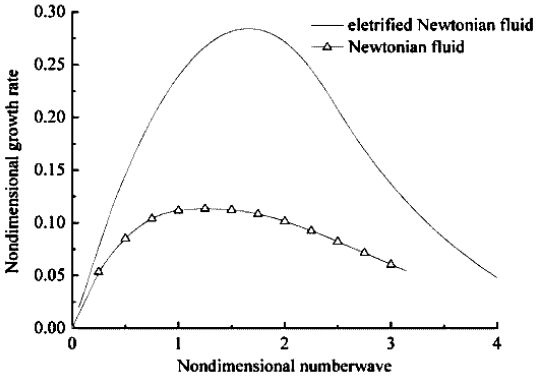

(a)

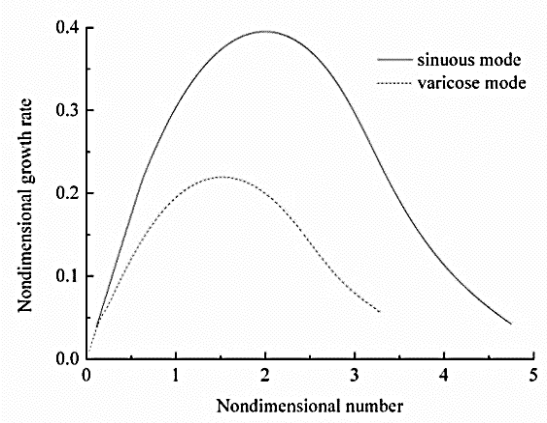

(b)

Fig. 3. Effects of the electrical Euler number

3.3 Effect of the Liquid Reynolds Number

Figures 5 and 6 show the effect of the Reynolds number of the liquid and gas on the disturbance wave growth rate by increasing the Re_1 from 510 to 1020 with other parameters fixed to be Eu=1, l=1, Re_2=180, We=100, Q=0.001 for the electrified liquid sheet, and Eu=0 for the non-electrified liquid sheet, respectively. In Fig. 6, the gas Reynolds number is increased from 9 to 162 with other parameters held constant (Eu=1, l=1, We=100, Q=0.001, Re_1=1700 for the electrified liquid sheet, and Eu=0 for the non-electrified liquid sheet).

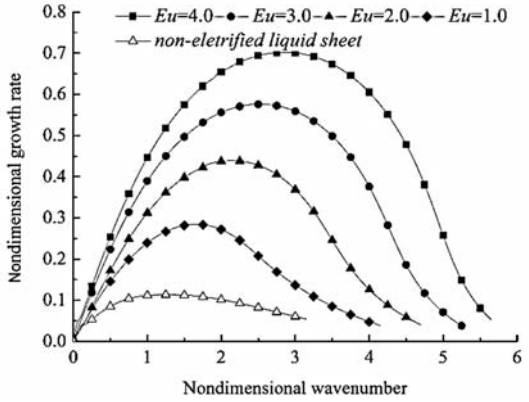

(a)

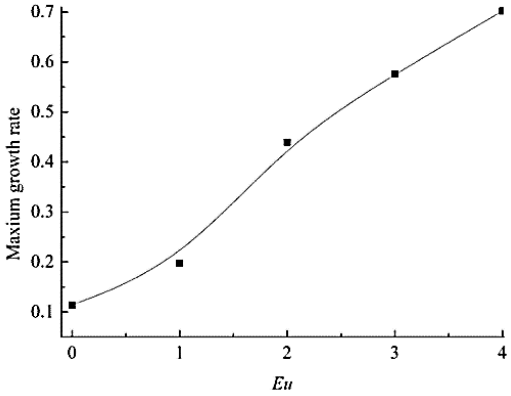

(b)

Fig. 4. Effects of the electrical Euler number

Figures 5 (b) and 6 (b) show that all the curves have a range in which the growth rate is positive. The maximum growth rate increases drastically with the increase in the electrified liquid Reynolds number, but the ambient gas Reynolds number have the opposite effect. The gas Reynolds number $Re_2 = U_2\delta\rho_2/\mu_2$ is reciprocally proportional to the liquid viscosity μ_2. The increase of the gas Reynolds number decreases with the increase of the gas viscosity. The physical mechanisms of the above trend are as follow: In present study, the liquid Reynolds numbers $Re_1 = U_1\delta\rho_1/\mu_1$ and the gas Reynolds numbers $Re_2 = U_2\delta\rho_2/\mu_2$ can be changed by varying the liquid velocity U_1 and gas velocity U_2, respectively. The gas-liquid relative velocity produced at the interface causes the aerodynamic instability. The larger gas-liquid relative velocity leads to a stronger aerodynamic interaction. In this case, the liquid sheets have more energy to overcome the liquid surface tension, viscosity dissipation and other factors, behave a greater instability. Therefore, the increase of the liquid Reynolds numbers and the decrease of the gas Reynolds numbers tend to accelerate the development of the disturbance waves.

In addition, the electrified liquid sheet is much more unstable than the non-electrified liquid sheet, as shown in Figs. 5 (a) and 6 (a). The results are the same as the forenamed analysis (Li (2011), Yang (2013)).

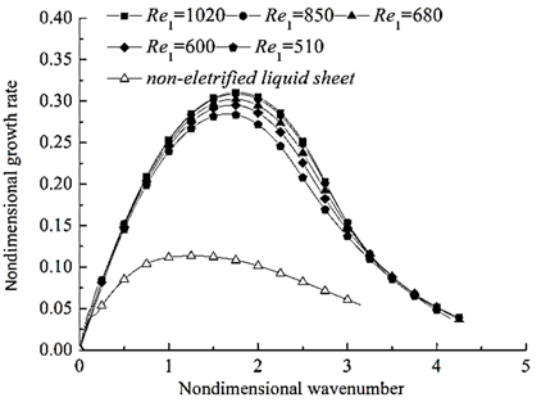

(a)

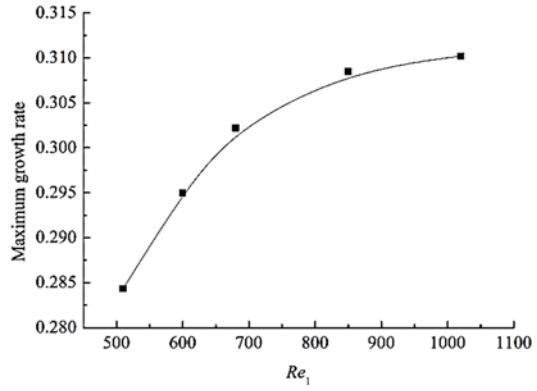

(b)

Fig. 5. Effects of the liquid Reynolds number

3.4 Effect of the gas-liquid density ratio

Figure 7 demonstrates the effect of the gas-liquid density ratio Q on the disturbance growth rate of the electrified liquid sheet by changing Q from 0.001 to 0.005, and other parameters kept constant to be Eu=1, Re_1=510, We=100, l=1 for the electrified liquid sheet, and Eu=0 for the non-electrified liquid sheet, respectively.

It is clear that the disturbance wave growth rate increases with the increase in the gas-liquid density ratio, and the liquid sheet of the electrified Newtonian liquid sheet is more unstable than that of the non-electrified liquid sheet in Fig. 7 (b). In the terms of physics, the gas-liquid density ratio Q is changed by changing the gas density. The aerodynamic instability at the interface becomes stronger with the increase of the gas density, which will make the electrified liquid sheet more unstable. Because the gas density increases with the increase of the gas pressure, a higher gas pressure can promote the breakup of the liquid sheet. The similar results were obtained by Liu *et al*. (1998).

Moreover, from the inspection of Fig. 7 (a), the disturbance of the electrified liquid sheet is more unstable than that of the non-electrified liquid sheet.

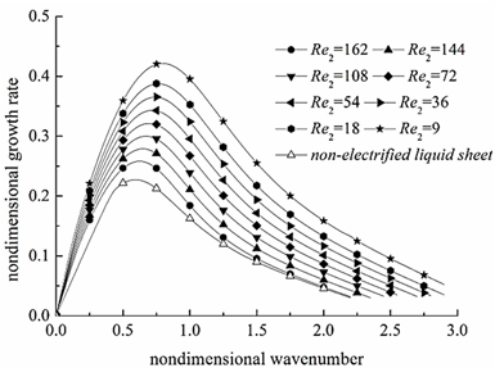

(a)

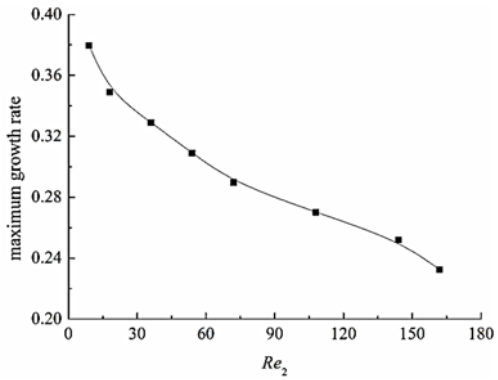

(b)

Fig. 6. Effects of the gas Reynolds number

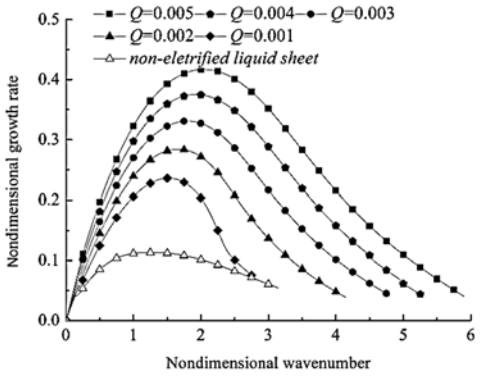

(a)

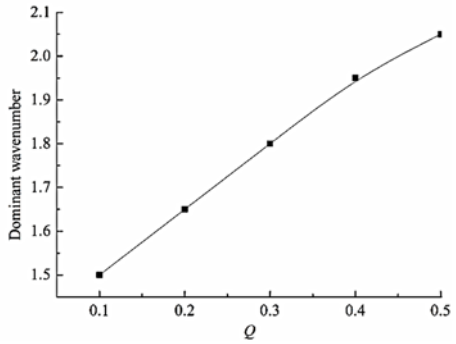

(b)

Fig. 7. Effects of the gas-liquid density ratio

3.5 Effect of the Weber number

The effect of the Weber number on the disturbance wave is described in Fig. 8 (a). Five values are calculated with other parameters invariable Eu=1, l=1, Re_1=510, Q=0.001 for the electrified liquid sheet, and Eu=0 for the non-electrified liquid sheet, respectively. The variation of the maximum growth rate is plotted in Fig. 8 (b). The disturbance wave growth rate increases with the increase of the liquid Weber number. The physical mechanisms of the above trend are as follows: The Weber number is directly proportional to the thickness of the liquid sheet, the Weber number increases with the increase of the liquid sheet thickness. Therefore, a thicker sheet is more unstable. Moreover, the Weber number is changed by varying the liquid surface tension, which resists the occurrence and development of the instability. The maximum growth rate increases with the decrease of the surface tension, and the breakup of the electrified liquid sheet will require less energy. Consequently, the increase of the Weber number enhances the occurrence and development of the electrified liquid sheet. It will take shorter time for the electrified liquid sheet to breakup.

Furthermore, the instability range increases with the increase of the Weber number.

3.6 Effect of Length

Figure 9 (a) show the effect of the ratio of distance between the horizontal electrode and liquid sheet to the liquid sheet thickness on the disturbance growth rate by varying l from 0.7 to 1.2 with other parameters invariable Eu=1, We=100, Re_1=510, Q=0.001 for the electrified liquid sheet, and Eu=0 for the non-electrified liquid sheet, respectively.

From the inspection of Fig. 9 (b), it is obvious that the maximum growth rate increases substantially with the decrease of the ratio l. In the terms of physics, the strength of the electrical field decreases with the increase in the distance of horizontal electrode δ, which is directly proportional to the ratio l. Consequently, the strength of the electrical field becomes weak with the increase in the ratio l. It can be concluded that a higher l damps the breakup of the electrified liquid sheet.

Moreover, from the inspection of Fig. 9 (a), the disturbance of the electrified liquid sheet is more unstable than that of the non-electrified liquid sheet.

3.7 Convergence Verification

The spectral method which is fast convergence and high accuracy is used for solving the eigenvalue problems of the instabilities and other mechanics problems (Orszag, 1971; Peyret, 2002). Equations (43-51) can be solved by the Chebyshev spectral method. To verify the method convergence, the calculate values N were chosen from 20 to 200 with keeping other parameters constant (Re_1=850, l=1, We=100, and MFR=0.27)). The growth rates are converged with the increase of the values N (N is amount of calculation), as shown in Fig. 10. When N=60, a series of good convergent results have been shown in Fig.10. N=200 is adopted in this paper.

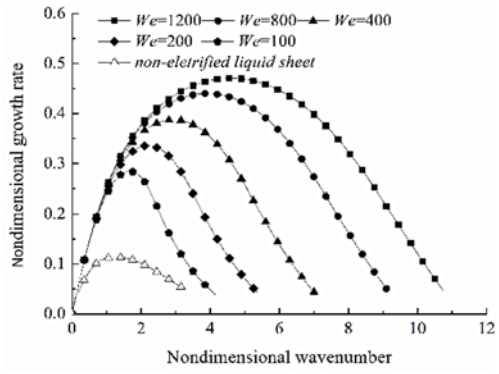

(a)

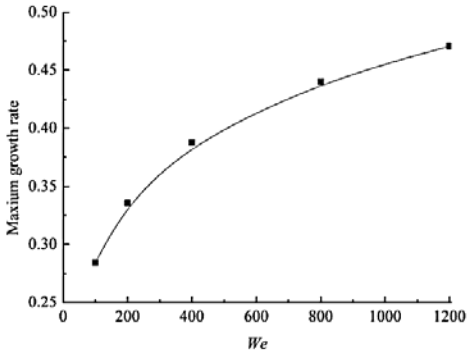

(b)

Fig. 8. Effects of the Weber number

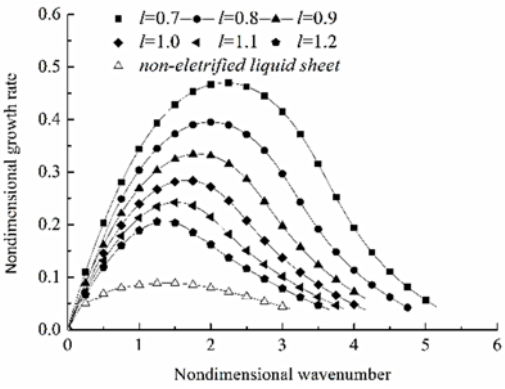

(a)

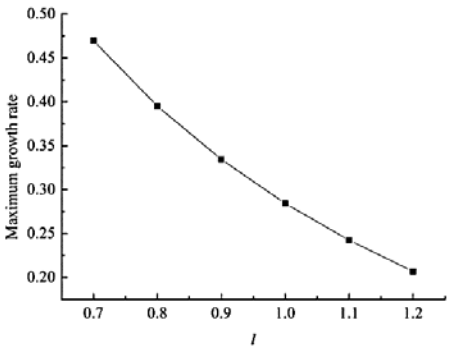

(b)

Fig. 9. Effects of *l*.

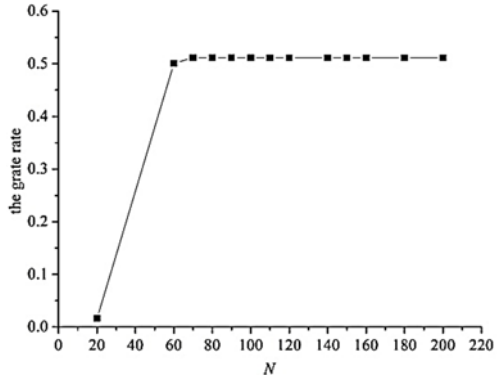

Fig. 10. Effect of *N* on growth rate

4. CONCLUSION

In this paper, the temporal instabilities of the electrified liquid sheets are investigated. The liquid sheets are surrounded by a viscous gas between two vertical parallel electrodes. As a novel contribution, the liquid and gas velocity profiles are considered. The effect of various parameters on the maximum growth rates has been obtained by solving the governing equations, which are used to investigate the breakup mechanism of the electrified liquid sheets.

As a result of the linear analysis described above, some conclusions may be drawn as follows:

1. For all parameters, the maximum growth rate of the electrified liquid sheets is much more unstable than that of the non-electrified liquid sheets.
2. The maximum growth rates of the sinuous mode are much higher than that of the varicose mode.
3. The increase of electrical Euler number, liquid Reynolds number, Weber numbers and gas-liquid density ratio can promote the breakup of the electrified liquid sheets.
4. The ratio of the distance between the horizontal electrode and the liquid sheet to the liquid sheet thickness and the ambient gas Reynolds number can restrain the breakup of the electrified liquid sheets.

ACKNOWLEDGEMENT

The financial support of China National Nature Science Funds (Support No. 51276055) the Tianjin Science and Technology Project (No. 14ZCDZGX0O821), the Hebei applied basic research project (No.13964308D) and the Hebei Young Science Funds (No. QN2017050) are gratefully acknowledged.

REFERENCES

Dombrowski, N. and Johns, W. R. (1963). The aerodynamic instability and disintegration of viscous liquid sheets, *Chemical Engineering Science.*, 18 203-214.

Duan, R., Chen Z. and Li L., (2014) Linear stability anslysis of an electrified viscoelastic liquid sheet in a viscous gas medium, *Atomization Spray* 24 155-179.

Fu, Q., Yang, L., Qu, Y., Gu B. (2010) Linear stability analysis of a conical liquid sheet, *Journal of Propulsion and Power* 26 955-968.

Georgiou, E., Papageorgiou, D. T., Maldarell, C., and Rumschitzki, D. S. (1991). Electrohydrodynamic stability of a annular electrolyte film surrounding a dielectric core in a tube, *Journal of Fluid Mechanics* 226, 149.

Grandison, S., Papageorgiou, D. T., Vanden-Broeck, J. (2007). Interfacial capillary waves in the presence of electric fields, *European Journal of Mechanics B/Fluids* 26 404-421.

Hagerty, W. W. and Shea, J. F. (1955). A study of the stability of plane fluid sheets, *Journal of Applied Mechanics* 22 509-514.

Ibrahim, E. A. (1998). Instability of a liquid sheet of parabolic velocity profile, *Physics of Fluids*, 10 1034-1036.

Lee, D. S. (2002). Nonlinear Instability of an Electrohydrodynamic Planar Jet, *Journal of Physical Science* 57 682-688.

Li, F., Liu, Z., Yin, X. and Yin, X. (2007). Theoretical and experimental investigation on instability of a conducting liquid jet under a radial electric field, *Chinese Quarterly of Mechanics*, 28 517-520.

Li, F., Yin, X. and Yin, X. (2011). Axisymmetric and non-axisymmetric instability of an electrically charged viscoelastic liquid jet [J]. *Journal of Non-Newtonian Fluid Mechanics*, 166 1024-1032

Li, X. (1993). Spatial instability of plan liquid sheets, *Chemical Engineering Science* 48 2973-2981.

Li, X. and Tankin, R.S. (1991) On the temporal instability of a two-dimensional viscosity liquid sheet *Journal of Fluid Mechanics* 226 425-443

Lin, S. P., Lian, Z. W. and Creighton, B. J. (1990). Absolute and convective instability of a liquid sheet, Journal of Fluid Mechanics, 220 673-689.

Liu, Z., Brenn, G. and Durst, F. (1998). Linear analysis of the instability of two-dimensional non-Newtonian liquid sheets, *Journal of Non-Newtonian Fluid Mechanics* 78 133-166.

Lozano, A. and Barreras, F. (2001) Longitudinal instabilities in an air-blasted liquid sheet, *Journal of Fluid Mechanics* 437 143-173.

Orszag, S. A. (1971). Accurate solution of the Orr-Sommerfeld stability equation, *Journal of Fluid Mechanics* 50 689-703.

Ozen, O., Papageorgiou, D. T., and Petropoulos, P. G. (2006).

Nonlinear stability of a charged electrified viscous liquid sheet under the action of a horizontal electric field, *Physics of Fluids* 18, 042102

Peyret, R. (2002). *Spectral Methods for Incompressible Viscous Flow* Springer New York Chap. 3

Savart, F. (1833) Mémoire sur le choc d'une veine liquide lancée contre un plan circulaire, In *Ann. de Chim*., 54 56-87.

Savettaseranee, K., Papageorgiou, D. T., Petropoulos, P. G., Tilley, B. S. (2003). The effect of electric fields on the rupture of thin viscous films by van der Waals forces, *Physics of Fluids* 15 641-652.

Shen, J. and Tang, T. (2006) *Spectral and high-order methods with applications* Science Beijing Chap. 2

Squire, H. B. (1953) Investigation of the instability of a moving liquid film, *British Journal of Applied Physics* 4 167-169.

Papageorgiou, D. T., Vanden-Broeck, J. M. (2004) Large-amplitude capillary waves in electrified fluid sheets, *Journal of Fluid Mechanics* 508, 71-88.

Taylor, G. I. (1959) *The dynamics of thin sheets of fluid. II. Waves on fluid sheets*, Proc. R. Soc. London Ser. A, 253 296-312.

Teng, C. H., Lin, S. P. and Chen, J. N. (1997). Absolute and convective instability of a viscous liquid curtain in a viscous gas, *Journal of Fluid Mechanics* 332 105-120.

Tilley, B. S., Petropoulos, P. G. and Papageorgiou, D. T. (2001). Dynamics and rupture of planar electrified liquid sheets, *Physics of Fluids* 13,3547-3563

Tomotika, S. (1935). On the instability of a cylindrical thread of a viscous liquid surrounded by another viscous fluid, *Proc. R. Soc*. London, Ser.,150,322-337.

Yang, L., Liu, Y. and Fu, Q. (2013). Linear Stability Analysis of an Electrified Viscoelastic Liquid Sheets. *Atomization sprays*, 20, 951-982.